

Reduced Order Transonic Aeroelastic Gust Response Simulation of Large Aircraft

P. Bekemeyer* and S. Timme†

University of Liverpool, Liverpool, England L69 3GH, United Kingdom

Reduced order modelling of large civil aircraft under gust excitation in transonic flight is discussed to enable computational fluid dynamics for routine gust load analysis. The impact of the elastically deforming structure is captured by tracing eigenmodes which originate in the structure, using the Schur complement method. Such global aeroelastic modes are computed for a case with nearly 48 million degrees of freedom. The gust response behaviour of the same full order system is sampled by computing complex-valued sinusoidal gust responses at several discrete frequencies. Modes representing the gust influence are obtained from the proper orthogonal decomposition technique which solves a small eigenvalue problem correlated to the sampling data. Afterwards, both sets of modes are combined and the linearised operator of the Reynolds-averaged Navier–Stokes equations is projected onto the coupled subspace. The obtained reduced order model can be solved in a rapid fashion to investigate various gust parameters.

I. Introduction

The investigation of aircraft responses to atmospheric turbulence is a crucial part during the aircraft design process since maximum gust loads are critical for wing sizing. A wide range of different parameters, e.g. gust shape and length, need to be investigated. Thus, low cost methods which offer highly accurate results are desired to ensure an accurate prediction of loads within an affordable time frame. Traditionally, linear aerodynamics in frequency domain, mostly the doublet lattice method,¹ are used to obtain forces rapidly. Examples for this are widespread from isolated wings² to full aircraft configurations.³ Whereas compressibility effects are accounted for, non-linear aerodynamic behaviour, such as shocks and boundary layer separation, is neglected even though these are inevitable at transonic flight conditions where nearly all modern aircraft operate. Two options are common to overcome this known lack of accuracy. Correction factors, either from experiments or computational fluid dynamics (CFD), can be applied after calculating linear aerodynamic forces to increase accuracy.⁴ While this method nearly retains the computational efficiency of the underlying linear potential method, correction factors are based on sampling only a few frequencies and modes using CFD. Nevertheless, correcting aerodynamic loads is the current industrial standard. The second option is analysing responses using CFD only,^{5,6} which predicts loads with increased accuracy also at nonlinear conditions. Unfortunately, computational cost of time-accurate simulations is still prohibitive during an industrial loads process.

A promising approach to reduced computational cost of CFD simulations, and thus to make it available in the aircraft loads process, is reduced order modelling (ROM).⁷ Model reduction based on system eigenmodes was initially used in combination with linear aerodynamics⁸ but has also gained interest within fluid dynamics.⁹ Considering a coupled fluid-structure problem, the Schur complement method can be applied to track structural eigenmodes while being affected by linearised CFD aerodynamics.¹⁰ Critical eigenmodes can be used in a centre manifold reduction to investigate transonic aeroelastic limit cycle oscillations and perform parameter sensitivity analysis.¹¹ While excellent agreement between results from the full nonlinear system and ROM is observed for free response, results are not as satisfying during gust excitation.¹² More recently, the authors proposed a modal extension to overcome this lack of accuracy by including additional modes representing the gust response characteristics of the system.¹³

*Ph.D. Student, School of Engineering; philipp.bekemeyer@liverpool.ac.uk.

†Lecturer, School of Engineering; sebastian.timme@liverpool.ac.uk.

A second, commonly used model reduction technique is based on proper orthogonal decomposition (POD).¹⁴ It allows the creation of a reduced basis for problems of very large size because the system behaviour is sampled rather than the characteristics of the system Jacobian matrix are investigated, which quickly becomes computationally prohibitive for industry relevant cases. POD was first used in fluid dynamics to model coherent structures in turbulent flow fields.¹⁵ A small eigenvalue problem, related to snapshots generated by numerically analysing the full system, is solved to obtain modes. This approach was soon extended towards frequency-domain sampling data from an incompressible three-dimensional vortex lattice method.¹⁶ Linearised CFD aerodynamics were first considered to analyse the dynamic response of a pitch-plunge aerofoil.¹⁷ More recently, an application for gust responses has been presented for an aerofoil in sub- and transonic flow conditions,¹³ showing excellent agreement at two orders of magnitude reduced computational cost. Combining POD with a linearised frequency-domain method not only reduces computational cost further, but, more importantly, an interpolation for frequencies not pre-computed can be avoided and a stable time-domain model is readily available. Results have also been presented for a large civil aircraft in cruise conditions.¹⁸

This paper enriches an eigenmode decomposition (EMD) ROM with POD modes to increase the prediction accuracy for loads occurring during transient gust responses of an aeroelastic aircraft. The construction of the EMD ROM is first discussed and mode traces are analysed. The lack of accuracy for gust responses is demonstrated for a 1-cos gust. A POD model is then introduced and both modal sets are combined. Responses of the coupled ROM are compared with full-order model (FOM) simulations for integrated quantities, structural deformations and surfaces pressures. Finally, computational cost for creating and solving the ROM is discussed.

II. Theoretical Formulation

A. Introducing Linearised Aerodynamics

The full-order nonlinear system is first presented. The state-space vector \mathbf{w} of size n can be written as

$$\mathbf{w} = [\mathbf{w}_f^T, \mathbf{w}_s^T]^T \quad (1)$$

where \mathbf{w}_f and \mathbf{w}_s denote fluid and structural degrees of freedom, respectively. While the size of \mathbf{w}_s is $O(100)$ using a modal structural model, the fluid degrees-of-freedom can be many millions. The governing equation in semi-discrete form is

$$\frac{d\mathcal{V}\mathbf{w}}{dt} = \mathbf{R}(\mathbf{w}, \mathbf{v}_g) \quad (2)$$

where \mathbf{R} is the nonlinear residual corresponding to the unknowns and \mathbf{v}_g denotes external disturbances due to gusts. The diagonal matrix \mathcal{V} contains the cell volumes for fluid degrees of freedom and an identity matrix for the structure. The difference between an equilibrium solution \mathbf{w}_0 and the state-space vector \mathbf{w} is introduced as

$$\Delta\mathbf{w} = \mathbf{w} - \mathbf{w}_0 \quad (3)$$

and accordingly for external disturbances \mathbf{v}_g and the cell volume matrix \mathcal{V} . The residual in Eq. (2) is expressed around the equilibrium point by a first-order Taylor expansion assuming small motions

$$\mathcal{V}\Delta\dot{\mathbf{w}} = \mathbf{R}(\mathbf{w}_0, \mathbf{v}_{g0}) + \frac{\partial\mathbf{R}}{\partial\mathbf{w}}\Delta\mathbf{w} + \frac{\partial\mathbf{R}}{\partial\mathbf{v}_g}\Delta\mathbf{v}_g \quad (4)$$

where $\frac{\partial\mathbf{R}}{\partial\mathbf{w}} = A$ denotes the coupled Jacobian matrix which can be partitioned just as the state-space vector as

$$A = \begin{bmatrix} A_{ff} & A_{fs} \\ A_{sf} & A_{ss} \end{bmatrix} \quad (5)$$

Note that changes in the cell volume $\mathbf{w}_0\mathcal{V}$ are contained within the matrix part A_{fs} to simplify the notation.¹⁹ The term $\mathbf{R}(\mathbf{w}_0, \mathbf{v}_{g0})$ in Eq. (4) represents the steady-state solution and is assumed to be zero.

B. Evaluating Basis from Eigenmodes

Right and left eigenvectors ϕ_i and ψ_i of the system Jacobian matrix A are calculated by solving the eigenvalue problems

$$A\phi_i = \lambda_i\phi_i \quad \text{and} \quad A^T\psi_i = \bar{\lambda}_i\psi_i \quad \text{for} \quad i = 1, \dots, m \quad (6)$$

for which the number m is far smaller than the initial system size n . Considering Eq. (5), the coupled direct eigenvalue problem can be rewritten as

$$A\phi_i = \begin{bmatrix} A_{\text{ff}} & A_{\text{fs}} \\ A_{\text{sf}} & A_{\text{ss}} \end{bmatrix} \phi_i = \lambda_i\phi_i \quad \text{and} \quad A^T\psi_i = \begin{bmatrix} A_{\text{ff}}^T & A_{\text{sf}}^T \\ A_{\text{fs}}^T & A_{\text{ss}}^T \end{bmatrix} \psi_i = \bar{\lambda}_i\psi_i \quad \text{for} \quad i = 1, \dots, m \quad (7)$$

where also the eigenvector ϕ_i is partitioned just as the state-space vector in fluid and structural contributions. The adjoint operation follows accordingly. The Schur complement method is used to determine eigenmodes by tracking structural modes while they are affected by the fluid. Thus, it is assumed that eigenvalues of interest are not eigenvalues of the aerodynamic block A_{ff} . Therefore, the small nonlinear eigenvalue problems can be solved for right and left eigenvalues

$$S(\lambda_i)\phi_{\text{s},i} = \lambda_i\phi_{\text{s},i} \quad \text{and} \quad S^T(\lambda_i)\bar{\psi}_{\text{s},i} = \lambda_i\bar{\psi}_{\text{s},i} \quad (8)$$

where the matrix $S(\lambda_i)$ is the Schur complement of A_{ff} in A

$$S(\lambda) = A_{\text{ss}} - A_{\text{sf}}(A_{\text{ff}} - \lambda\mathcal{V})^{-1}A_{\text{fs}} \quad (9)$$

Newton's method is applied to solve Eq. (8) using structural frequencies as an initial guess to the eigenvalue.¹⁰

Computational cost is reduced by precomputing the term $(A_{\text{ff}} - \lambda\mathcal{V})^{-1}A_{\text{fs}}$ at a small number of reduced frequencies for all structural modes of interest. An interpolation surrogate model is then applied during Newton's method to obtain aerodynamic forces.²⁰ Whereas the structural entries of ϕ_i and ψ_i are readily available after solving Eq. (8), the aerodynamic entries need an additional linear system solve using the eigenvalue as a complex shift.

Collecting the eigenvectors, the right and left modal matrices are formed as

$$\Phi_{\text{EMD}} = [\phi_1, \dots, \phi_m, \bar{\phi}_1, \dots, \bar{\phi}_m] \quad \text{and} \quad \Psi_{\text{EMD}} = [\psi_1, \dots, \psi_m, \bar{\psi}_1, \dots, \bar{\psi}_m] \quad (10)$$

Because structural eigenvalues appear as complex conjugate pairs, these are added to the model basis at no additional cost. Furthermore, the eigenvectors are normalised to fulfil the biorthonormality condition

$$\Psi_{\text{EMD}}^H \mathcal{V} \Phi_{\text{EMD}} = I \quad (11)$$

C. Evaluating Basis from Proper Orthogonal Decomposition Modes

First, K snapshots at discrete reduced frequencies ω^* , normalised using the freestream velocity U_∞ and the reference chord length l_{ref} , are generated solving the linear system

$$(A_{\text{ff}} - i\omega^*\mathcal{V})\hat{\mathbf{w}}_{\text{f}} = -\frac{\partial \mathbf{R}_{\text{f}}}{\partial \mathbf{v}_{\text{g}}}\hat{\mathbf{v}}_{\text{g}}(\omega^*) \quad (12)$$

with $\hat{\mathbf{w}}$ and $\hat{\mathbf{v}}$ as complex-valued Fourier coefficients, assuming that $\Delta \mathbf{w}$ and $\Delta \mathbf{v}_{\text{g}}$ change harmonically in time.²¹ Solutions $\hat{\mathbf{w}}_{\text{f}}$ are stored as columns in the snapshot matrix S as

$$S = [\hat{\mathbf{w}}_{\text{f},1}, \dots, \hat{\mathbf{w}}_{\text{f},K}, \bar{\hat{\mathbf{w}}}_{\text{f},1}, \dots, \bar{\hat{\mathbf{w}}}_{\text{f},K}] \quad (13)$$

The POD basis Φ_{POD} is obtained as a linear combination of snapshots

$$\Phi_{\text{POD}} = SV \quad (14)$$

where the columns of V are scaled so that vectors in Φ_{POD} are unit length. The eigenvalue problem of dimension K

$$S^H \mathcal{V} S \mathbf{v}_j = \mu_j \mathbf{v}_j \quad \text{for} \quad j = 1, \dots, K \quad (15)$$

is solved to ensure the best possible approximation in Eq. (14). Note, that the dot product has been altered by considering the matrix \mathcal{V} .²² Whereas the previously introduced EMD-based ROM is unaffected by this change in dot product, the characteristics of the POD model change. First, cells with a small volume are becoming less important resulting in a more global flowfield representation. Second and more importantly, the resulting POD model is most likely to be stable compared with the case excluding \mathcal{V} . Eigenvalues μ_k are real and positive because $S^H \mathcal{V} S$ is a Hermitian matrix. The relative information content contributed to the system by a certain mode, also often referred to as energy, is given by

$$r_k = \mu_k \left(\sum_{i=0}^K \mu_i \right)^{-1} \quad (16)$$

This can be used to decrease the number of modes further by only considering those with a high relative information content.

D. Combined Model Basis and Model Reduction

An aeroelastic ROM is introduced to investigate the influence of gust excitations on flexible structures by combining the two bases just introduced as

$$\Phi = [\Phi_{\text{EMD}}, \Phi_{\text{POD}}] \quad \text{and} \quad \Psi = [\Psi_{\text{EMD}}, \Psi_{\text{POD}}] \quad (17)$$

where $\Psi_{\text{POD}} = \Phi_{\text{POD}}$. Only the aerodynamic subsystem is considered to identify Φ_{POD} and thus all POD modes are padded with zero entries in the structural part to match the dimensions of the coupled system.

Describing the change in state-space vector $\Delta \mathbf{w}$ by

$$\Delta \mathbf{w} = \Phi \mathbf{z} \quad (18)$$

and substituting in Eq. (4), gives after performing a Petrov-Galerkin projection

$$\Psi^H \mathcal{V} \Phi \dot{\mathbf{z}} = \Psi^H A \Phi \mathbf{z} + \Psi^H \frac{\partial \mathbf{R}}{\partial \mathbf{v}_g} \Delta \mathbf{v}_g \quad (19)$$

Since biorthonormality is no longer fulfilled for the coupled model, the inverse of $\Psi^H \mathcal{V} \Phi$ is pre-multiplied resulting in the time-domain representation of the coupled reduced order model

$$\dot{\mathbf{z}} = (\Psi^H \mathcal{V} \Phi)^{-1} \Psi^H A \Phi \mathbf{z} + (\Psi^H \mathcal{V} \Phi)^{-1} \Psi^H \frac{\partial \mathbf{R}}{\partial \mathbf{v}_g} \Delta \mathbf{v}_g \quad (20)$$

While multiplying with the inverse changes the projection based on Ψ , the reduction described by Φ remains unchanged. Solving the reduced system in either frequency or time domain, and reconstructing full order solutions afterwards, is an efficient way to investigate gust encounter for coupled fluid-structure systems.

E. Computational Fluid Dynamics Method

Aerodynamics are solved using the DLR-TAU code which is widely used in the European aerospace sector and validations of the code are available in the literature for steady^{23,24} as well as unsteady cases.^{24,25} The RANS equations in conjunction with the Spalart–Allmaras turbulence model²⁶ are solved. Inviscid fluxes are discretised applying a central scheme with the scalar artificial dissipation of Jameson, Schmidt and Turkel.²⁷ Exact gradients used for viscous and source terms are computed using the Green–Gauss approach. Steady-state solutions are obtained using the backward Euler method with lower-upper Symmetric–Gauss–Seidel iterations²⁸ and local time-stepping. Convergence is accelerated by applying a 2v multigrid scheme.

Structural deformations are considered using a modal approach. The surface deformations of both, bending and torsion dominated modes, multiplied by a scaling factor for better visualisation, are shown in Fig. 1 together with the undeformed surface. Arising volume mesh deformations are calculated by the DLR-TAU code applying the radial basis function method.²⁹ Gusts are modelled using the field velocity approach which introduces an artificial mesh velocity.³⁰ The velocity term is added to the governing equations and is prescribed based on the gust excitation while no additional deformation of the computational grid is required. The gust parameters are visualised in Fig. 2.

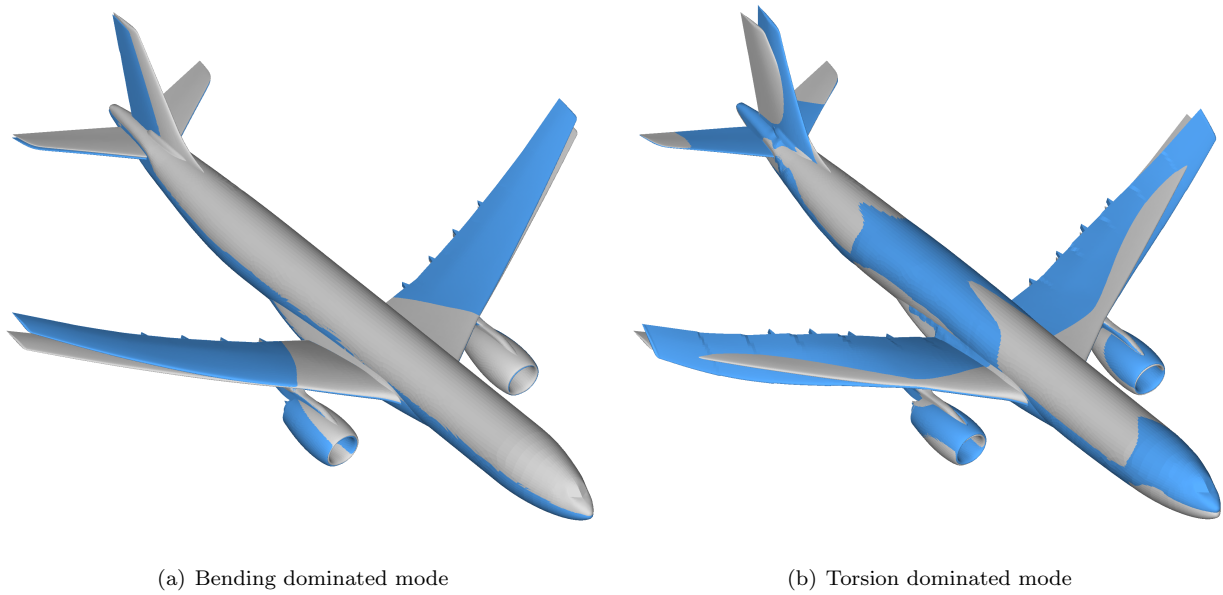


Figure 1. Representative mode shapes projected on the CFD surface mesh with the undeformed surface in light grey

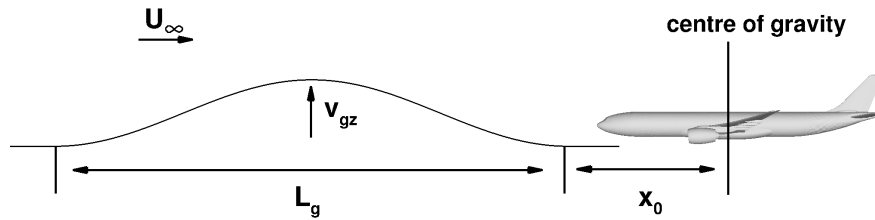


Figure 2. Sketch of gust parameters

Abort density residual	10^{-3}
Non-dimensional time-step size	0.1
Number of time steps	1500
Number of subiterations	5

Table 1. Time-domain numerical parameters

During unsteady simulations aerodynamic and structural systems are solved separately from each other and data is exchanged on a subiteration level.³¹ Subiterations at each time-step are performed until the euclidean norm of the generalised-force update drops below 10^{-4} or a maximum number of 5 is reached. For the aerodynamic system a dual time-stepping combined with the second-order backward differentiation formula is used, settings of which are summarised in Table 1. Time-step size and number of time steps follow from numerical experiments. Further, a Cauchy convergence criterion with a tolerance of 10^{-8} for the relative error of the drag coefficient is applied in addition to an abort criterion based on the density residual. The structural system is integrated in time applying the Newmark-beta method.³²

The linearised frequency-domain formulation is based on a first-discretise-then-linearise, matrix-forming approach with an analytical, hand-differentiated Jacobian matrix. A generalised conjugate residual solver with deflated restarting is used to solve arising linear systems.³³ For preconditioning a block incomplete

Number of Krylov vectors	80
Number of deflation vectors	20
Abort density residual	10^{-7}

Table 2. Frequency-domain numerical parameters

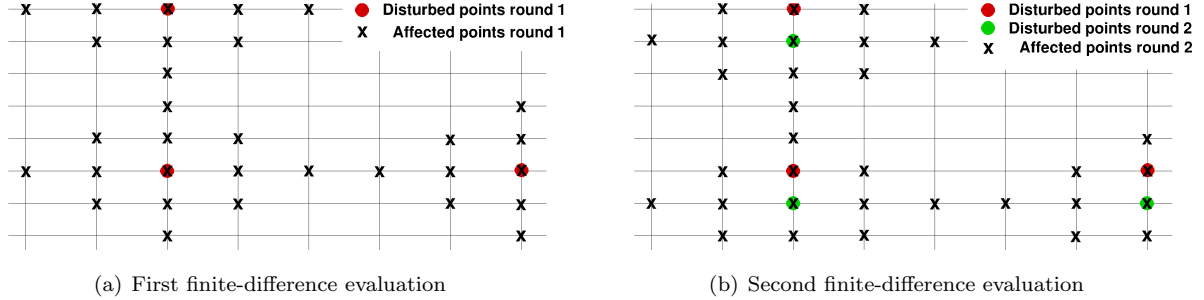


Figure 3. Demonstration of finite-difference approach for forming $\partial\mathbf{R}/\partial\mathbf{v}_g$

lower-upper factorisation of the Jacobian matrix with zero level of fill-in is applied.³⁴ The number of Krylov and deflation vectors employed to solve linear systems together with the linear convergence criterium are given in Table 2 and are based on previously published results.³³

F. Numerical Aspects

The matrix $\partial\mathbf{R}/\partial\mathbf{v}_g$ in Eq. (20) is formed using a central finite-difference approach

$$-\frac{\partial\mathbf{R}}{\partial\mathbf{v}_g} = \frac{\partial\mathbf{R}}{\partial\dot{\mathbf{x}}} = \frac{\mathbf{R}(+\varepsilon\dot{\mathbf{x}}) - \mathbf{R}(-\varepsilon\dot{\mathbf{x}})}{2\varepsilon} \quad (21)$$

since an analytical derivation is currently missing. Computational cost is reduced by disturbing grid-point velocities of all points that are neither first nor second neighbour of another disturbed point. The set of disturbed points defines the columns of the matrix, while the resulting non-zero residual entries define the rows. For a second-order accurate scheme this procedure is demonstrated on a Cartesian grid in Fig. 3. Following a first finite-difference evaluation shown in Fig. 3(a), a new set of, as yet undisturbed, grid points is selected. This procedure is repeated until all points have been disturbed once. Depending on the partitioning applied, between 190-230 finite-difference evaluations are required for the presented test case to construct the full matrix. Note that, even though the procedure is demonstrated using a Cartesian grid, the computational grid of the test case is hybrid.

Since a linear Taylor expansion is used, the assumption of a dynamically linear response also extends to integrated quantities, such as lift and moment coefficient. Thus, changes in global coefficients, e.g. ΔC_L , can be computed by forming the partial derivative $\partial C_L/\partial\mathbf{w}$ and then substituting the expression in Eq. (18)

$$\Delta C_L = \frac{\partial C_L}{\partial\mathbf{w}} \Delta\mathbf{w} = \frac{\partial C_L}{\partial\mathbf{w}} \Phi\mathbf{z} \quad (22)$$

This enables the analysis of global coefficients without the need of reconstructing the surface solution from the ROM data.

III. Results

The chosen test case is a large civil aircraft in cruise flight. The computational mesh consists of nearly 8 million points. A steady-state solution at a Mach number of 0.85 and an altitude of 10 km is obtained using an elastic trimming procedure based on Broyden's method,³⁵ which balances lift and weight while ensuring zero pitching moment. The steady simulation includes 94 structural modes to represent elastic deformation

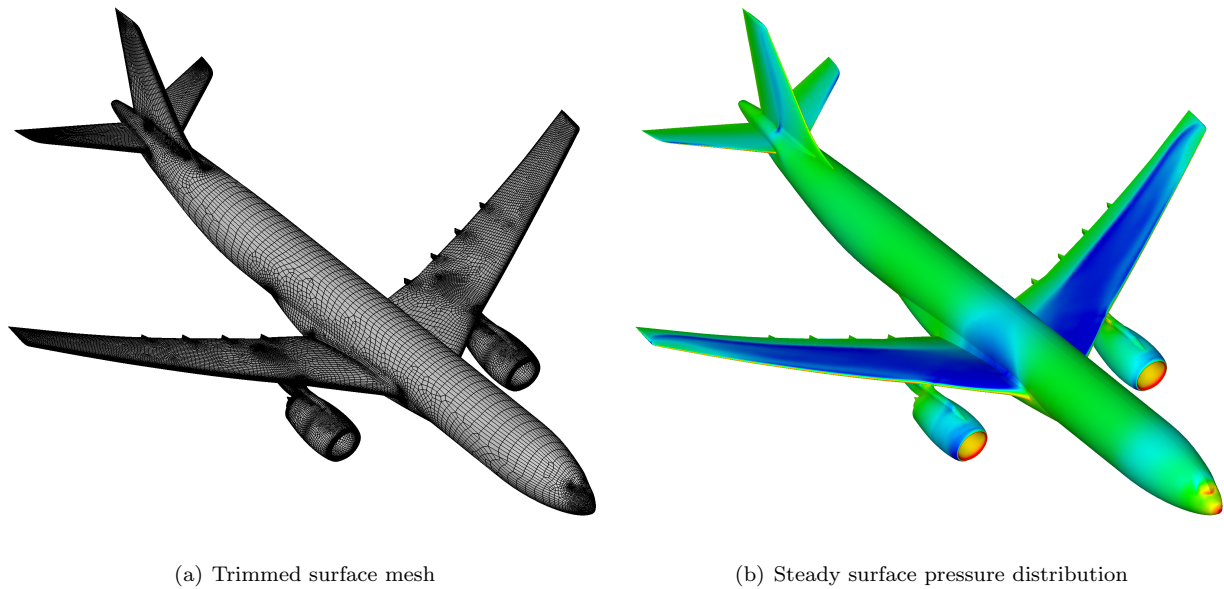


Figure 4. Trimmed surface mesh and steady-state surface pressure coefficient

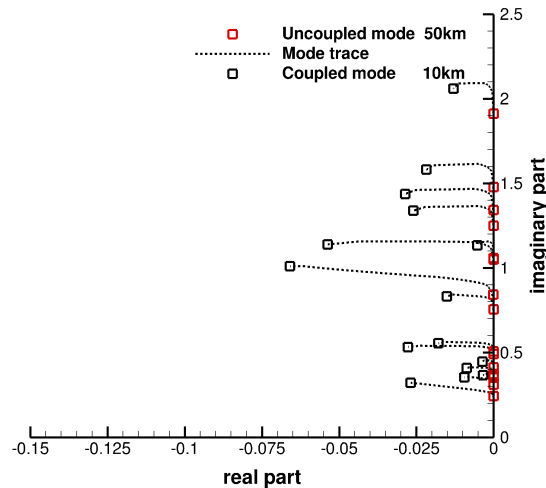


Figure 5. Change in real and imaginary part for 15 eigenmodes over altitude

while for trimming an artificial mode for the elevator deflection is used. The elevator deflection and angle of attack are iteratively adjusted until the desired aerodynamic coefficients are reached. The final surface mesh, after driving the density residual to converge seven orders of magnitude, is visualised in Fig. 4(a). A strong shock along the wingspan at roughly 70% chord length can be seen in the steady surface pressure distribution in Fig. 4(b). Furthermore, the effects of the first wing bending mode in conjunction with the torsion mode cause a decrease of sectional lift towards the wing tip. The elevator is deflected during the trimming process resulting in a strong suction area around the leading edge but no shock formation.

The 15 highest amplified structural modes are identified during the steady trimming process and considered in the following for dynamic responses. Aerodynamic responses of these structural modes are sampled at 12 reduced frequencies between 0 and 2. No structural damping is considered. The evolution of the structural eigenvalues whilst affected by the fluid is then traced solving Eq. (8) at a starting altitude of 50 km until the target altitude of 10 km is reached. Resulting mode traces are shown in Fig. 5. With

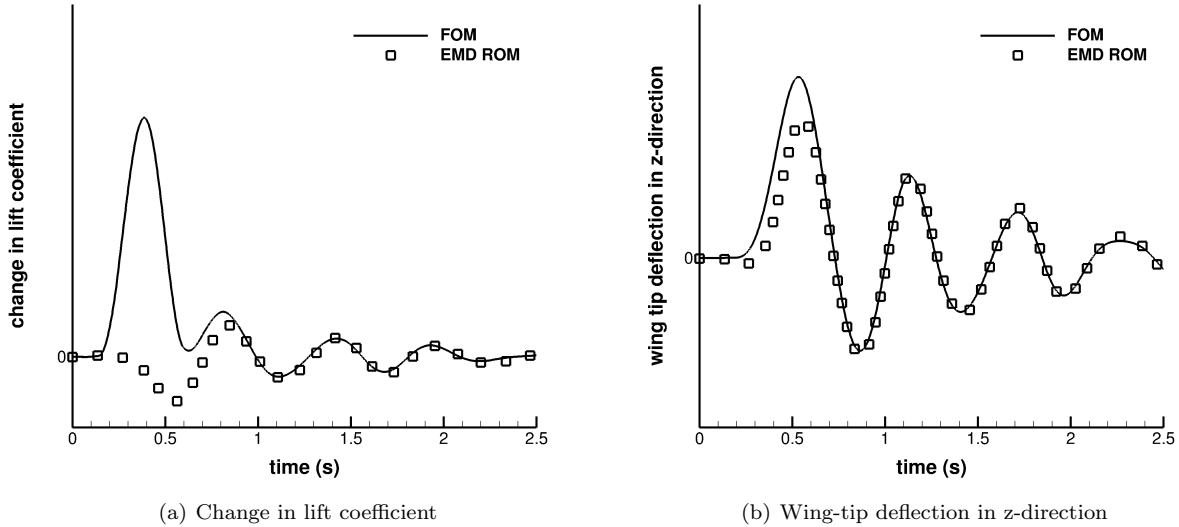


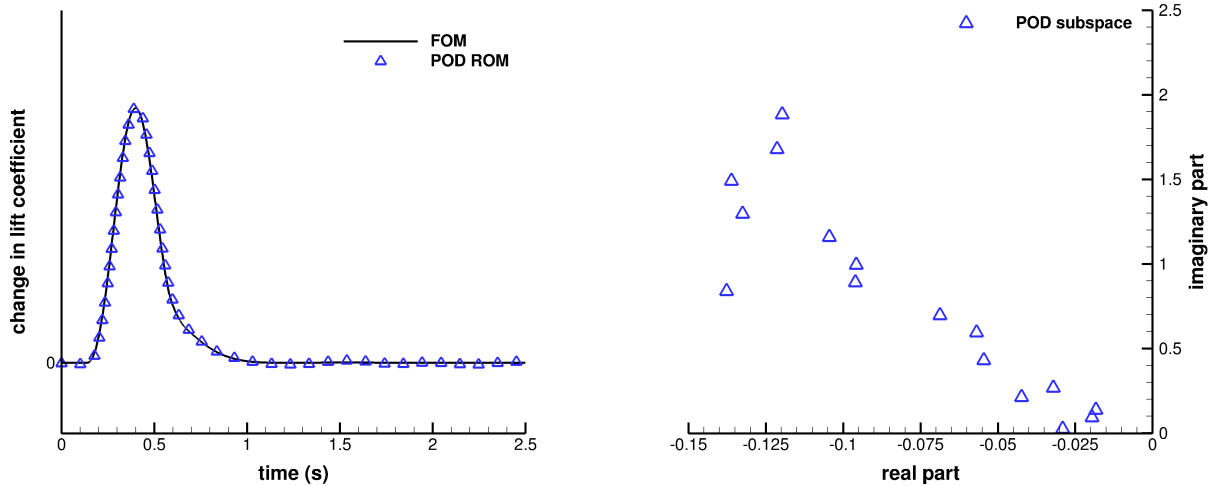
Figure 6. Gust response of EMD-based ROM for 1-cos gust with $L_g = 116$ m

decreasing altitude the density increases and thus the coupling between aerodynamic and structural forces becomes stronger. This coupling causes all modes to deviate from the imaginary axis towards a negative real part. Left and right eigenvectors are computed, discarding the real part of the eigenvalue, just as the initial p-k-type sampling, when solving for the aerodynamic part. As outlined in Sec. II B complex-conjugates of all modes are included at no additional cost. Subsequently, the coupled Jacobian and gust influence matrices are reduced and projected onto the model basis to reduce the system size from 48 million to only 30 degrees of freedom.

Next, the generated EMD ROM is used to investigate the gust response of the flexible aircraft rapidly. The gust parameters are $L_g = 116$ m, $v_{gz} = 0.01 \times U_\infty$ and $x_0 = 5 \times l_{ref}$, which is a medium gust length considering the certification requirements for large civil aircraft.³⁶ The small amplitude is chosen to ensure a dynamically linear response of the time-marching solution. The changes in lift coefficient and wing tip displacement in z-direction are displayed in Figs. 6(a) and 6(b), respectively. The ROM is not capable of reproducing the lift build-up due to the gust excitation, which effectively introduces an increment in angle of attack. However, once the gust is past the aircraft and the change in lift is dominated by the damped structural response, the FOM and ROM predict a similar response. This behaviour can also be observed for the wing tip deflection even though not as distinct.

In principle, the accuracy of responses to external excitation, such as gust, can be increased by enriching the modal basis with modes originating in the aerodynamic block A_{ff} of the coupled Jacobian matrix. In fact, this is common for ROMs based on linear potential theory or even more simplistic using Küssner and Wagner aerodynamics for a pitch-plunge aerofoil.³⁷ The problem of this approach in combination with CFD-level aerodynamics is twofold. The size of the Jacobian matrix directly correlates with the mesh size as well as the number of conservative variables. For the presented case this results in approximately 48 million degrees of freedom and thus determining all eigenvalues and a-posteriori selecting the eigenvalues of interest, is computationally prohibitive. Instead, computing a small number of eigenmodes for such problems is possible as demonstrated for stability analyses.^{38–40} However, for these approaches a region of interest needs to be defined a-priori which is currently not understood for gust responses. Thus, including eigenmodes from A_{ff} is considered not feasible and instead a subspace is approximated in the following using POD based on linearised responses of the aircraft to gust excitation.

The gust response of the aerodynamic subsystem is sampled at 20 reduced frequencies, again between 0 and 2. Results and their corresponding complex-conjugates are used as snapshots to construct a POD ROM as outlined in Sec. II C. The retained energy r_k is set to 99.99% resulting in 39 POD modes. Analysing the same gust parameters as for Fig. 6, the change in lift coefficient for a full-order, rigid aircraft gust response simulation and the POD ROM is shown in Fig. 7(a) with good agreement. Some minor deviations are visible



(a) Change in lift coefficient to gust with $L_g = 116$ m (b) Eigenspectrum of reduced fluid Jacobian matrix

Figure 7. POD-based ROM characteristics

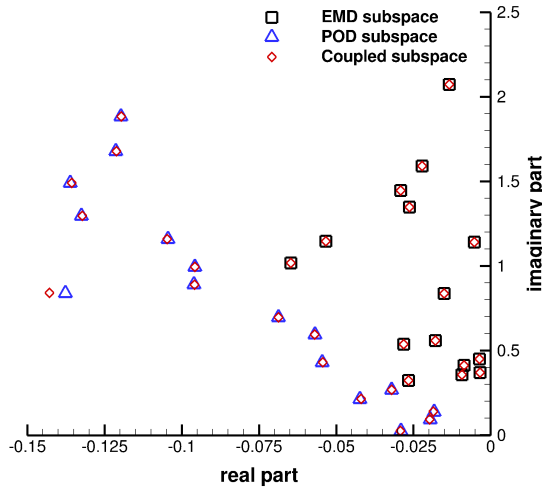
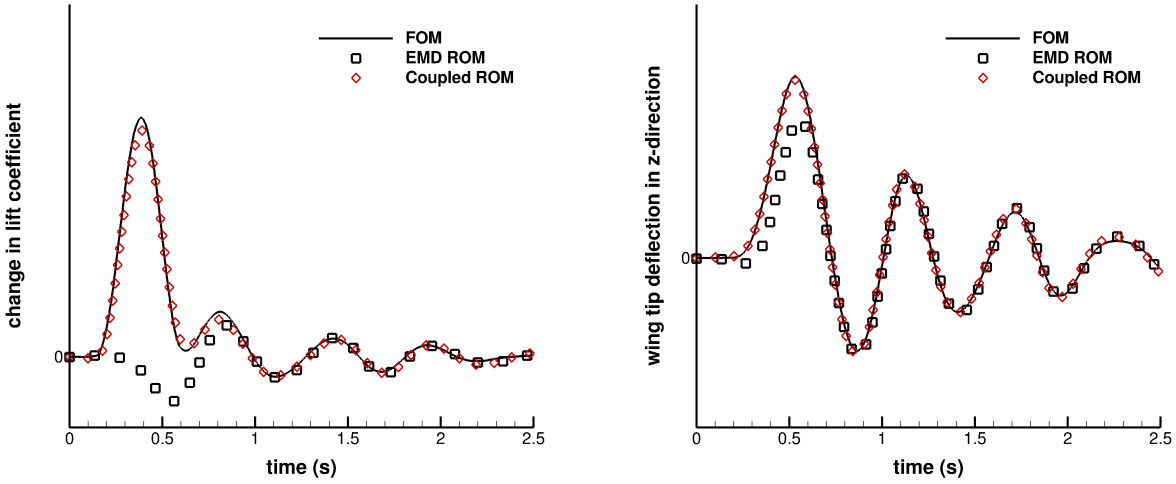


Figure 8. Eigenspectrum of reduced Jacobian matrix for POD, EMD and coupled ROM

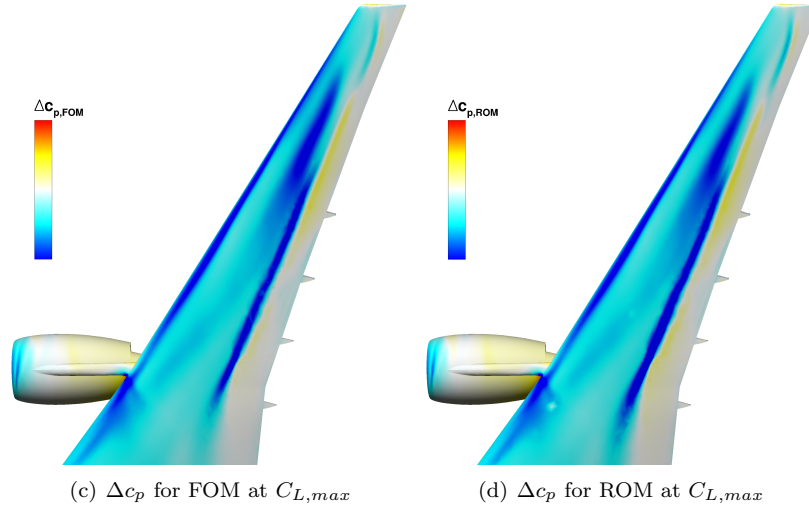
in the ROM response after the gust has passed the aircraft, which is a result of the sampled frequency range. A more detailed discussion of the POD ROM for this particular case, including pressure distributions for the first mode and responses to different gust lengths, has been presented previously.¹⁸ Part of the eigenspectrum of the fluid Jacobian matrix projected onto the POD modes, $\Psi_{\text{POD}}^H A_{\text{ff}} \Phi_{\text{POD}}$, is displayed in Fig. 7(b). It was demonstrated in [17] for a significantly smaller case that this eigenspectrum is an approximation of the full-order eigenspectrum of A_{ff} . In fact, the outer shape of the eigenspectrum is clearly visible.

Both modal bases are combined by using the technique outlined in Sec. II D. Part of the coupled eigenspectrum, together with both individual solutions, is displayed in Fig. 8. The dimension of the coupled ROM is 69 which is significantly smaller than the FOM with nearly 48 million. The influence of the multiplication with $(\Psi^H \mathcal{V} \Phi)^{-1}$ is expected to be small since the diagonal entries are one, due to $\Psi_{\text{EMD}}^H \mathcal{V} \Phi_{\text{EMD}} = I$ and $\Psi_{\text{POD}}^H \mathcal{V} \Phi_{\text{POD}} = I$. However, some eigenvalues, which are originating from POD modes, experience a slight shift in real part whereas the imaginary part remains mostly unchanged. EMD-based eigenvalues are



(a) Change in lift coefficient

(b) Wing-tip deflection in z-direction



(c) Δc_p for FOM at $C_{L,max}$

(d) Δc_p for ROM at $C_{L,max}$

Figure 9. Gust response of coupled ROM for 1-cos gust with $L_g = 116$ m

basically unaffected by the coupling. The coupled formulation now contains the subspace of both individual ROMs and thus is capable of predicting a coupled fluid-structure response subject to gust excitation.

The coupled ROM is now used to investigate the same gust parameters as in Fig. 6. The changes in lift coefficient and wing tip displacement in z-direction are shown in Figs. 9(a) and 9(b), respectively. For both quantities of interest an improvement is observed. The ROM correctly predicts the change in lift coefficient while the gust is above the aircraft. Some minor differences occur around the peak value and during the transition from an aerodynamically dominated response to structural dominated behaviour around $t = 0.7$ s. The wing tip deflection shows an even better improvement making the FOM and ROM nearly indistinguishable. The ROM not only offers global coefficients and structural degrees of freedom at greatly reduced cost but also the flow topology of the whole domain. Thus, the change in surface pressure at the peak lift value is displayed in Figs. 9(c) and 9(d) for the FOM and ROM, respectively. Overall good agreement is observed with some minor differences close to the wing tip and in the engine-pylon-wing junction region. Based on the presented surface pressures, quantities of interest during the aircraft loads process, such as sectional loads and root wing bending moments, are readily accessible.

Once the ROM is verified for a single 1-cos gust, arbitrary gust lengths can be analysed at negligible additional computational cost. Dynamic responses for the change in lift coefficient for two representative gust lengths of $L_g = 18$ m and 214 m, are visualised in Fig. 10(a). Excellent agreement between the reduced

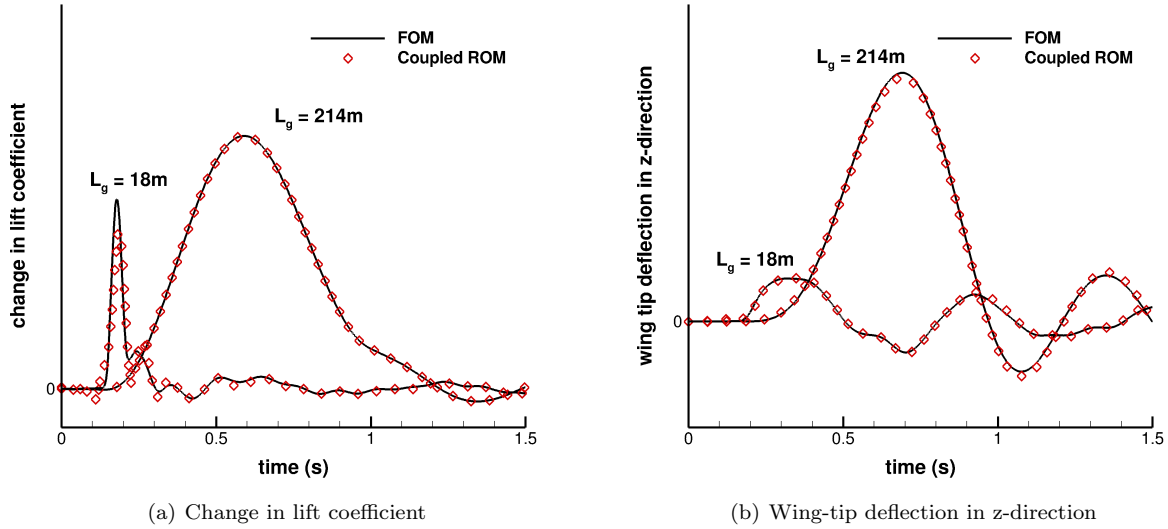


Figure 10. Gust responses of coupled ROM for 1-cos gusts with $L_g = 18\text{ m}$ and $L_g = 214\text{ m}$

Offline Tasks		192 cores	Cost
Time-domain simulation (single 1-cos response)			47 h
Reduced order model construction			120 h
a) Sampling EMD basis			107 h
b) Sampling POD basis			13 h
c) Constructing coupled ROM			$\ll 1\text{ h}$
Online Tasks		1 core	Cost
Reduced order model solving			7 min
Rebuilding global coefficients			$\ll 1\text{ min}$
Rebuilding surfaces pressure distributions			$\ll 1\text{ min}$

Table 3. Comparison of computational cost for aircraft case

model and the full order reference solutions is obtained for the longer gust length. Minor differences occur around maximum lift for the shorter gust length. Adding sampling data also at higher reduced frequencies for the POD ROM will increase the accuracy of the coupled ROM also for shorter gust lengths. However, the dynamic response of the wing tip deflection in Fig. 10(b) shows good agreement between the full and reduced model.

Computational cost is summarised for the FOM and ROM in Tab. 3. Timings were obtained on the UK based high power computing facility ARCHER^a using 192 standard compute cores. Since the computational time for a time-domain 1-cos simulation depends on the investigated gust length, the time listed with 47 h is an average of all three presented gust responses. The time of 120 h for the ROM generation contains the time needed for producing all sampling data and the subsequent coupled model construction. Solving the ROM can afterwards be done on a single core desktop computer and requires roughly 7 minutes, again slightly depending on the gust length of interest. It should be noted that roughly 95% of this time is needed for forming the matrix vector product $\Psi^H \frac{\partial \mathbf{R}}{\partial \mathbf{v}_g} \Delta \mathbf{v}_g$ since this is performed over the full-order dimension. Further reduction can be investigated in the future. Reconstruction of global coefficients, surface pressure distributions and structural deformations is negligible. Also, as demonstrated above, the ROM can be used

^aAdvanced Research Computing High End Resource

to investigate a wide range of gust parameters without recomputing it, assuming the frequency range of interest is covered. Thus, the ROM method offers a speed-up factor compared to time-marching, coupled fluid-structure simulations if more than 2 different sets of gust parameters are of interest. Based on the acceptable means of compliance,⁴¹ published together with the certification requirements, around 30 different sets of gust parameters are of interest at one flight point which results in a speed up factor of one order of magnitude using the ROM approach presented herein.

IV. Conclusions

This paper outlines a method to compute coupled fluid-structure responses to gust encounter at reduced computational cost while preserving the accuracy of the underlying computational fluid dynamics solver. Structural deformations are accounted for by considering aeroelastic eigenmodes which originate from the structure. This model is then extended by adding proper orthogonal decomposition modes to enhance the prediction accuracy during gust encounter. Following the model reduction, a large number of gust responses can be obtained at negligible computational cost on a local desktop machine.

The presented test case is an elastically-trimmed passenger aircraft at transonic flight conditions. First, global direct and adjoint eigenmodes are calculated for this industry-relevant test case with nearly 48 million degrees of freedom using the Schur complement formulation. Secondly, the gust response behaviour of the aerodynamic system is sampled in the frequency domain and subsequently a proper orthogonal decomposition model is constructed. Both modal bases are then combined and a coupled model is created by accounting for the non-existing biorthonormality. The resulting dimension of the small-sized system is 69 and thus a significant reduction is achieved compared to nearly 48 million. Coupled gust responses are compared to time-marching simulations for several quantities of interest, including change in lift coefficient, wing tip deflection and instantaneous surface pressure distributions, with good agreement. Finally, computational cost is discussed to evaluate the efficiency gain provided from the proposed model reduction.

Additional snapshots at higher reduced frequencies should be included in the aerodynamic proper orthogonal decomposition model to increase the accuracy for short gust lengths. Further, the influence of the pk-style sampling, neglecting aerodynamic damping, on the eigenmode model should be investigated by fully solving the Schur formulation. The efficiency of the reduced order model can be increased further by also reducing the size of the matrix $\Psi^H \frac{\partial \mathbf{R}}{\partial \mathbf{v}_g}$ by applying e.g. a multigrid technique.

Acknowledgements

The research leading to these results was co-funded by Innovate UK, the UK’s innovation agency, as part of the Enhanced Fidelity Transonic Wing project. This work used the ARCHER UK National Supercomputing Service (<http://www.archer.ac.uk>).

References

- ¹Albano, E. and Rodden, W. P., “A Doublet Lattice Method for Calculating Lift Distribution on Oscillating Surfaces in Subsonic Flow,” *AIAA Journal*, Vol. 7, No. 2, 1969, pp. 279–285.
- ²Giesing, J. P., Rodden, W. P., and Stahl, B., “Sears Function and Lifting Surface Theory for Harmonic Gust Fields,” *Journal of Aircraft*, Vol. 7, 1970, pp. 252–255.
- ³Kier, T., “Comparison of Unsteady Aerodynamic Modelling Methodologies with Respect to Flight Loads Analysis,” *AIAA Atmospheric Flight Mechanics Conference and Exhibit*, 2005, AIAA Paper 2005-6027.
- ⁴Dimitrov, D. and Thormann, R., “DLM-Correction Methods for Aerodynamic Gust Response Prediction,” *International Forum on Aeroelasticity and Structural Dynamics (IFASD)*, 2013, IFASD Paper 2013-24C.
- ⁵Raveh, D. E., “CFD-Based Models of Aerodynamic Gust Response,” *Journal of Aircraft*, Vol. 44, No. 3, 2007, pp. 888–897.
- ⁶Reimer, L., Ritter, M., Heinrich, R., and Krüger, W., “CFD-based Gust Load Analysis for a Free-flying Flexible Passenger Aircraft in Comparison to a DLM-based Approach,” *22nd AIAA Computational Fluid Dynamics Conference*, 2015, AIAA Paper 2015-2455.
- ⁷Lucia, D. J., Beran, P. S., and Silva, W. A., “Reduced-order modeling: new approaches for computational physics,” *Progress in Aerospace Sciences*, Vol. 40, No. 1-2, 2004, pp. 51–117.
- ⁸Bisplinghoff, R. L., Ashley, H., and Halfman, R. L., *Aeroelasticity*, Dover Publications, 1955.
- ⁹Taira, K., Brunton, S. L., Dawson, S. T. M., Rowley, C. W., Colonius, T., McKeon, B. J., Schmidt, O. T., Gordeyev, S., Theofilis, V., and Ukeiley, L. S., “Model Analysis of Fluid Flows: An Overview,” *AIAA Journal*, 2017, accepted for publication.

- ¹⁰Badcock, K. J. and Woodgate, M. A., “Bifurcation Prediction of Large-Order Aeroelastic Models,” *AIAA Journal*, Vol. 48, No. 6, 2010, pp. 1037–1046.
- ¹¹Woodgate, M. A. and Badcock, K. J., “Fast prediction of transonic aeroelastic stability and limit cycles,” *AIAA Journal*, Vol. 45, No. 6, 2007, pp. 1370–1381.
- ¹²Timme, S., Badcock, K. J., and Da Ronch, A., “Linear Reduced Order Modelling for Gust Response Analysis using the DLR-TAU Code,” *International Forum on Aeroelasticity and Structural Dynamics (IFASD)*, 2013, IFASD Paper 2013-36A.
- ¹³Bekemeyer, P. and Timme, S., “Reduced Order Gust Response Simulation using Computational Fluid Dynamics,” *57th AIAA/ASCE/AHS/ASC Structures, Structural Dynamics, and Materials Conference*, 2016, AIAA Paper 2016-1485.
- ¹⁴Dowell, E. H. and Hall, K. C., “Reduced Order Models in Unsteady Aerodynamic Models, Aeroelasticity and Molecular Dynamics,” *ICAS - 26th Congress of International Council of the Aeronautical Sciences*, 2008, ICAS 2008-0.1.
- ¹⁵Lumley, J. L., “The Structures of Inhomogeneous Turbulent Flow,” *Atmospheric Turbulence and Radio Wave Propagation*, 1967, pp. 166–178.
- ¹⁶Kim, T., “Frequency-Domain Karhunen-Loève Method and Its Application to Linear Dynamic Systems,” *AIAA Journal*, Vol. 36, No. 11, 1998, pp. 2117–2123.
- ¹⁷Hall, K. C., Thomas, J. P., and Dowell, E. H., “Proper Orthogonal Decomposition Technique for Transonic Unsteady Aerodynamic Flows,” *AIAA Journal*, Vol. 38, No. 10, 2000, pp. 1853–1862.
- ¹⁸Bekemeyer, P., Thormann, R., and Timme, S., “Rapid Gust Response Simulation of Large Civil Aircraft using Computational Fluid Dynamics,” *RAeS Applied Aerodynamics Conference*, 2016.
- ¹⁹Thormann, R. and Widhalm, M., “Linear-Frequency-Domain Predictions of Dynamic-Response Data for Viscous Transonic Flows,” *AIAA Journal*, Vol. 51, No. 11, 2013, pp. 2540–2557.
- ²⁰Timme, S., Marques, S., and Badcock, K. J., “Transonic aeroelastic stability analysis using a kriging-based schur complement formulation,” *AIAA Journal*, Vol. 46, No. 6, 2011, pp. 1202–1213.
- ²¹Bekemeyer, P., Thormann, R., and Timme, S., “Frequency-Domain Gust Response Simulation using Computational Fluid Dynamics,” *AIAA Journal*, 2017, accepted for publication.
- ²²Amsallem, D. and Farhat, C., *On the Stability of Reduced-Order Linearized Computational Fluid Dynamics Models Based on POD and Galerkin Projection: Descriptor vs Non-Descriptor Forms*, Springer International Publishing, 2014, pp. 215–233.
- ²³Schwamborn, D., Gerhold, T., and Heinrich, R., “The DLR TAU-Code: Recent Applications in Research and Industry,” *European Conference on Computational Fluid Dynamics*, 2006, ECCOMAS CFD 2006.
- ²⁴Stickan, B., Dillinger, J., and Schewe, G., “Computational aeroelastic investigation of a transonic limit-cycle-oscillation experiment at a transport aircraft wing model,” *Journal of Fluids and Structures*, Vol. 49, 2014, pp. 223–241.
- ²⁵Neumann, J. and Mai, H., “Gust response: Simulation of an Aeroelastic Experiment by a Fluid-Structure Interaction Method,” *Journal of Fluids and Structures*, Vol. 38, 2013, pp. 290–302.
- ²⁶Spalart, P. R. and Allmaras, S. R., “A One-Equation Turbulence Model for Aerodynamic Flows,” *Recherche Aérospatiale*, Vol. 1, 1994, pp. 5–21.
- ²⁷Jameson, A., Schmidt, W., and Turkel, E., “Numerical Solutions of the Euler Equations by Finite Volume Methods Using Runge-Kutta Time-Stepping Schemes,” *14th Fluid and Plasma Dynamic Conference*, 1981, AIAA Paper 1981-1259.
- ²⁸Dwight, R., “An Implicit LU-SGS Scheme for Finite-Volume Discretizations of the Navier-Stokes Equations on Hybrid Grids,” *DLR-FB-2005-05*, 2006.
- ²⁹Michler, A., “Aircraft control surface deflection using RBF-based mesh deformation,” *International Journal for Numerical Methods in Engineering*, Vol. 88, 2011, pp. 986–1007.
- ³⁰Parameswaran, V. and Baeder, J. D., “Indicial Aerodynamics in Compressible Flow-Direct Computational Fluid Dynamic Calculations,” *Journal of Aircraft*, Vol. 34, No. 1, 1997, pp. 131–133.
- ³¹Jirasek, A., M., D., and Navratil, J., “Computational Fluid Dynamics Study of Benchmark Supercritical Wing at Flutter Condition,” *AIAA Journal*, Vol. 55, No. 1, 2017, pp. 153–160.
- ³²Newmark, N. M., “A method of computation for structural dynamics,” *Journal of Engineering Mechanics*, Vol. 85, No. 3, 1959, pp. 67–94.
- ³³Xu, S., Timme, S., and Badcock, K. J., “Enabling off-design linearised aerodynamics analysis using Krylov subspace recycling technique,” *Computers and Fluids*, Vol. 140, 2016, pp. 385–396.
- ³⁴Saad, Y., *Iterative Methods for Sparse Linear Systems*, Society for Industrial and Applied Mathematics, Philadelphia, PA, 2nd ed., 2003.
- ³⁵Broyden, C. G., “A class of methods for solving nonlinear simultaneous equations,” *Mathematics of Computation (American Mathematical Society)*, Vol. 19, No. 92, 1965, pp. 577–593.
- ³⁶European Aviation Safety Agency, “Certification Specifications for Large Aeroplanes (CS-25),” 2015.
- ³⁷Tantaroudas, N., Da.Ronch, A., Gai, G., Badcock, K. J., and Palacios, R., “An Adaptive Aeroelastic Control Approach by using Nonlinear Reduced Order Models,” *14th AIAA Aviation Technology, Integration, and Operations Conference*, 2014, AIAA Paper 2014-2590.
- ³⁸Iorio, M. C., Gonzalez, L. M., and Ferrer, E., “Direct and adjoint global stability analysis of turbulent transonic flows over a NACA0012 profile,” *International Journal for Numerical Methods in Fluids*, Vol. 76, No. 3, 2014, pp. 147–168.
- ³⁹Sartor, F., Mettot, C., and Sipp, D., “Stability, receptivity and sensitivity analyses of buffeting transonic flow over a profile,” *AIAA Journal*, Vol. 53, No. 7, 2015, pp. 1980–1993.
- ⁴⁰Timme, S. and Thormann, R., “Towards Three-Dimensional Global Stability Analysis of Transonic Shock Buffet,” *16th AIAA Aviation Technology*, 2016, AIAA Paper 2016-3848.
- ⁴¹European Aviation Safety Agency, “Certification Specifications for Large Aeroplanes Amendment 17 (CS-25),” 2015.